

UHASSELT



Maastricht University

KNOWLEDGE IN ACTION

Faculty of Medicine and Life Sciences
School for Life Sciences

Master of Biomedical Sciences

Master's thesis

The influence of extracellular matrix cues on retinal pigment epithelium biomechanics in an aging model

Jonas Schimmel

Thesis presented in fulfillment of the requirements for the degree of Master of Biomedical Sciences, specialization
Molecular Mechanisms in Health and Disease

SUPERVISOR :

Prof. dr. Helena SLAETS

SUPERVISOR :

dr. Jacopo DI RUSSO

MENTOR :

drs. Teodora PISKOVA

Transnational University Limburg is a unique collaboration of two universities in two countries: the University of Hasselt and Maastricht University.



UHASSELT

KNOWLEDGE IN ACTION

www.uhasselt.be
Universiteit Hasselt
Campus Hasselt:
Martelarenlaan 42 | 3500 Hasselt
Campus Diepenbeek:
Agoralaan Gebouw D | 3590 Diepenbeek

2023
2024



Maastricht University

Faculty of Medicine and Life Sciences

School for Life Sciences

Master of Biomedical Sciences

Master's thesis

The influence of extracellular matrix cues on retinal pigment epithelium biomechanics in an aging model

Jonas Schimmel

Thesis presented in fulfillment of the requirements for the degree of Master of Biomedical Sciences, specialization
Molecular Mechanisms in Health and Disease

SUPERVISOR :

Prof. dr. Helena SLAETS

SUPERVISOR :

dr. Jacopo DI RUSSO

MENTOR :

drs. Teodora PISKOVA

The influence of extracellular matrix cues on retinal pigment epithelium biomechanics in an aging model

Jonas Schimmel¹, Teodora Piskova^{2,3,4}, Jacopo Di Russo^{2,3,4}

¹Hasselt University, Campus Diepenbeek, Agoralaan Gebouw C - B-3590 Diepenbeek

²Institute of Molecular and Cellular Anatomy, RWTH Aachen University, 52074 Aachen, Germany

³Interdisciplinary Centre for Clinical Research, RWTH Aachen University, 52074 Aachen, Germany

⁴DWI-Leibniz-Institute for Interactive Materials, 52074 Aachen, Germany

To whom correspondence should be addressed: Jacopo Di Russo, Tel: +49-241 80-89106; Email: jdirusso@ukaachen.de

Keywords: Biomechanics, Retinal pigment epithelium, Laminin, Aging, Tissue remodeling

ABSTRACT

Age-related macular degeneration (AMD) is a prevalent retinal disorder, affecting nearly 30% of the population over the age of 75. AMD is characterized by retinal pigment epithelium (RPE) degeneration and the remodeling of the RPE's extracellular matrix (ECM), including increased collagen crosslinking, reduced elastin content, and the formation of heterogeneous structures termed drusen. Understanding how biochemical cues and physical cues from the ECM tune RPE mechanics and function during the aging process is crucial for developing potential therapeutics. In this study, we present our novel approach to investigate the effect of ECM cues in an *in vitro* model of age-mimicking uncompensated apoptosis in post-mitotic hiPSC-derived RPE. Polyacrylamide hydrogels of 4 and 11 kPa, coated with ECM proteins laminin-332 or laminin-511, were used as culture substrates, providing different physical (stiffness) and biochemical (laminin isoform) ECM cues. RPE cells were transduced with a caspase-8-containing virus, allowing on-demand apoptosis induction to simulate RPE cell density reduction in aging. Our findings indicate that both physical and biochemical cues modulate structural, biomechanical, and functional RPE responses. Laminin-551 shows greater sensitivity to the substrates' physical cues than laminin-332. Nevertheless, laminin-332 drives changes in viscoelasticity. Furthermore, stiffer substrates generally led to more notable changes in cellular mechanics. Overall, these results provide valuable insights into the role of ECM cues for RPE mechanics in aging and the pathogenesis of diseases such as AMD.

INTRODUCTION

Features of the retinal pigment epithelium – The retinal pigment epithelium (RPE) is a monolayer, consisting of microvilli-covered cells (1-3). These cells are located in the outermost layer of the retina between photoreceptors and the Bruch's membrane (BrM) (1-3). The photoreceptors are responsible for light detection, while the BrM provides the extracellular matrix (ECM) (1-3). RPE cells lose their ability to undergo mitosis, therefore becoming post-mitotic (4). Due to this post-mitotic nature, RPE cell loss occurs with age, decreasing by approximately 0.3% per year, which is accompanied by an overall thinning of cells (5, 6). The RPE is a very versatile tissue, fulfilling multiple functions to retain eyesight such as the formation of the outer blood-brain barrier, providing transepithelial nutritional and waste transport, protection against scattered light, and phagocytosis and degradation of photoreceptor outer segments (POS) (2). The RPE supports the photoreceptors by being responsible for their homeostasis and development (2). With their long apical processes, they envelop the outer segments of photoreceptor cells (7). Photoreceptors frequently shed parts of their membranous discs at their distal ends, i.e., outer segments, which are phagocytized by the RPE and degraded by lysosomes within the RPE (8). Daily shedding accumulates to 5% of photoreceptor mass being internalized by the RPE (9).

Structural features of the RPE - The RPE shows a strong apical to basal polarization, which is important for proper functioning (10). As with any cell, the RPE has a cytoskeleton that is responsible for a platitude of functions such as structural stability, adhesion, motility, force transmission, and adapting the cell shape (11-13). The RPE cytoskeleton consists of several cytoskeletal molecules,

including microfilaments (i.e., F-actin), microtubules, and intermediate filaments, forming different but interconnected networks and their adhesions (14). Microfilaments are responsible for establishing polarity, microtubules for organelle movement, and keratin intermediate filaments for maintaining cell shape and rigidity (14). During aging, altered cell arrangement and extracellular drusen deposits, cause increased mechanical stress, in turn inducing structural changes that are compensated by actin stress fibers (15). At the cell-cell interface, multiple protein structures are present such as tight junctions, adherens junctions, and desmosomes, forming intercellular connections (16-18). Tight junctions form the closest intercellular barrier, allowing epithelial cells to act as a diffusion barrier through the intracellular space (19). Adherens junctions consist of major transmembrane proteins such as E-cadherins which pair between opposing cells, forming a bond (20). Adherens junctions function as cell-cell adhesion stabilizers, actin cytoskeleton regulators, and regulators of intracellular signaling and transcription (18). By being connected to the actin skeleton and being able to regulate it, adherens junctions can act as mechanosensors which ultimately influence biomechanics (21). Lastly, desmosomes couple adjacent cells which connect intracellularly with the intermediate filament cytoskeleton (17). By forming strong adhesion bonds and cytoskeletal linkages, a strong resistance to mechanical stress is provided (17).

Influence of cellular shape - The RPE is a simple monolayer with a variable cell shape throughout the retinal location and age. Healthy RPE cells located centrally near the fovea are predominantly hexagonal, uniform in size, and mononucleated (22). Further lateral on the visual axis, RPE cells change to larger, asymmetric, and more multinucleated cells (22). During aging, cells become more irregular, and enlarged (22). In pathological conditions, the degeneration process is fastened and may end in age-related macular degeneration (AMD) (22). Individual cell shape plays a collective role in cellular dynamics at the tissue level. Cell shape influences the jamming and unjamming of tissues (23). Jammed tissues act solid-like and are associated with tissue homeostasis, rigidity, and mechanical stability, while unjammed tissues are fluid-like and are associated with mechanical fluidity and plasticity (23). A jammed state allows for large mechanical changes, giving increased control over biomechanics and responsiveness to the environment (23). Cell-cell interactions allow increased cohesion, contributing to a more jammed state (24). Cell-substrate interactions additionally contribute to cell jamming via integrin-based traction forces (25). Here, increased cell-substrate adhesion causes cell spreading and provides an unjammed state (25). However, conflicting reports are present and the exact mechanisms are not known (23, 25).

Bruch's membrane in aging - Basal of the RPE lies the BrM, which is a connective tissue that forms a complex with the apical RPE, providing structural support, and helping with the diffusion of molecules (26). Aging, and to a greater extent pathological conditions such as AMD, cause extracellular deposit formation between the RPE and the BrM, called drusen (27). Additionally, the BrM undergoes fundamental changes such as thickening, changing of matrix molecules, and a decreased thickness of the elastic layer, increasing the overall stiffness (3, 28). BrM elasticity begins to decrease linearly from the age of 21 at an annual rate of 1% (29).

Cell-ECM adhesion - In addition to cell-cell adhesion, receptors such as integrin contribute to cellular connectivity at the cell-ECM interface (30, 31). Integrins are the main receptors binding and conveying signals from the extracellular matrix to the cell (32). They consist of two transmembrane glycoproteins, the α - and β subunits, which form heterodimers (33). 18 α and 8 β subunits genes are presently known, providing 24 different α , β combinations which thus far have been identified at the protein level (34). Depending on the composition of the heterodimer, various extracellular ligands can bind to the heterodimer, such as laminin, fibronectin, vitronectin, and collagen (33). Laminins are known to bind to a wide variety of integrin types, including $\alpha3\beta1$, $\alpha6\beta4$, $\alpha6\beta1$, $\alpha7\beta1$, and $\alpha10\beta1$ (34, 35). Laminins are glycoproteins consisting of three disulfide-linked polypeptides, divided into α , β , and γ chains (36). 11 distinct genes can be found in the human genome, coding for five α , three β , and three γ subunits (36). Depending on the subunit composition, nomenclature is determined, i.e., $\alpha1$, $\beta1$, and $\gamma1$ form laminin-111 (37). Not all laminin isoforms bind to every integrin heterodimer, $\alpha3\beta1$ and $\alpha6\beta4$ show clear specificity for laminin-332 and laminin-511, while $\alpha6\beta1$ shows broad specificity (38). Laminin isoform expression is age and tissue specific (39, 40). Laminin-511 is the most ubiquitous isoform in adults, while laminin-332 is only expressed in the basal lamina underlying epithelial cells (39, 40). When integrins cluster, they can establish different types of higher order adhesion structures,

one of the best described being focal adhesions, connecting the actin cytoskeleton to the extracellular matrix (41). Focal adhesions are regulated upstream by Rho, a Ras-related GTP-binding protein, which stimulates myosin contractility, ultimately leading to actin filament bundling and integrin aggregation (41).

Biomechanical properties of the RPE - Understanding adhesion dynamics is important for mechanobiology as it is an important link between extracellular influences, cellular adhesions, structure, and eventual function, building on the idea that mechanical changes can be important contributors, rather than only consequences of diseases development. One of the most significant factors inducing biomechanical changes are physical stimuli (42). Cells can sense physical stimuli such as substrate stiffness by mechanosensation, mechanotransduction, and mechanoresponses (43). Focal adhesions, which tether the cytoskeleton to the substrate, allow for the propagation of physical signals which are transformed into biochemical signals (43, 44). The cytoskeleton is linked to the nucleus, therefore signals can reach the nucleus by actin polymerization and microtubule assembly, inducing morphological changes, growth, or differentiation (43-45). These changes can influence biomechanical factors such as stiffness and viscoelastic properties of the cell. Stiffness measures the resistance of a material to deformation due to mechanical forces acting upon it (42). Cell stiffness, quantified as the Young's modulus, is a ratio of stress, determined by the amount of force per area unit applied by the cantilever, and strain, determined by how much the material was deformed by the applied force of the cantilever (46). With higher substrate stiffness, the state of the cytoskeleton changes, affecting cell volume and spread, thereby influencing the stiffness (42). The stiffness provided by the substrate and the tension generated by the cytoskeleton need to be in balance to maintain cell shape (47). Therefore, when increasing the substrate stiffness and disrupting the balance, cells will spread more on the substrate (48). A further biomechanical factor is viscoelasticity, which refers to the viscous and elastic properties when subjected to deformation (49). Viscoelasticity allows an architectural structure and a solid-like nature, while also allowing a more fluid-like nature for dynamic changes (49). Furthermore, viscoelasticity can help cells resist forces exerted by surrounding cells or substrates (42). When subjected to stiffer substrates, the elastic modulus increases more than the viscous modulus, showing reduced dampening abilities (42). A further factor influencing biomechanics is how cells engage and disengage their ECM binding sites, called the molecular clutch mechanism, which can be tuned by substrate stiffness (50, 51). Low-stiffness ECMs cause a slower loading rate compared to the total integrin-ECM bond lifetime, causing bond failure before force transmission. Meanwhile, stiffer ECM substrates cause faster clutch loading and ultimately exceed the total integrin-ECM bond lifetime, resulting in full force transmission. However, if the stiffness of the substrate is too high and above the optimal rigidity, clutch loading is too fast, resulting in destabilization and disengagement of the integrin-ECM bond, reducing total force transmission. Therefore, increasing substrate stiffness leads to increased traction forces generated by cells. Increased substrate stiffness and traction force are accompanied by additional focal adhesions and integrin clustering to maintain high force transmission (50, 52). Biochemical cues affect RPE contractility, which is modulated by the density of laminin and laminin isotype itself, with laminin-511 promoting higher contractility compared to laminin-332 (53). Increased contractility in the RPE is associated with reduced function of POS internalization (53).

Aim - In this paper, we aim to study the contribution of both physical cues, such as substrate stiffness, and biochemical cues, such as laminin isotypes, to the biomechanical properties of RPE cells in aging and the possible link to functional improvement or decline.

EXPERIMENTAL PROCEDURES

Glass activation – The surface of 20 mm glass bottom dishes (Cellvis, D35-20-0-N) or 6-well dishes (Cellvis, P061.5HN) were chemically activated to ensure covalent polyacrylamide (PAA) gel attachment. This process involved initial exposure to a 0.1M NaOH (Merck, 1.06498.1000) solution for 5 minutes, followed by a 4% (3-Aminopropyl)triethoxysilane (APTS) (Sigma Aldrich, 440140) - isopropanol (VWR, 20.942.330) solution for 5 minutes, and finally, immersion in 1% glutaraldehyde (Merck, 354400) in ddH₂O for 30 minutes.

Hydrogel preparation – PAA hydrogels of either a 4kPa or 11kPa stiffness were prepared. 4kPa gels were prepared with a mixture of 0.1% Bis (Bio-Rad, 1610142), 5% Acrylamide (Bio-Rad, 1610140) - phosphate buffered saline (PBS), while 11kPa gels were prepared with a mixture of 0.07%

Bis, 10% Acrylamide/PBS. Polymerization was initiated by using 1:200 10% ammonium persulfate (APS) (Sigma, 248614-5G) and 1:2000 tetramethylethylenediamine (TEMED) (Bio-rad, 1610800). Coverslips were placed on a 3D-printed mold where the hydrogel solution was pipetted. Glass bottom dishes were placed upside down onto the coverslips and the hydrogel was allowed to polymerize at room temperature. After polymerization, the coverslips were removed and gels were cut with a 4 mm biopsy puncher (PFM Medical, B451851) and trimmed with tweezers.

Covalent functionalization - Gels were covalently functionalized with ECM proteins by degassing a solution of water, 0.5M HEPES (Carl Roth, 9105.4), 100% ethanol (Sigma, 1070172511), and 0.2% Bis-acrylamide (Bio-Rad, 161-0142) for 20 minutes followed by adding 0.2 v/v% Tetramethacrylate (Sigma, 408360) in ethanol, 0.03% N-hydroxysuccinimide ester (Sigma, A8060) in a 50% ethanol, and 3% 2-Hydroxy-4'-(2-hydroxyethoxy)-2-methylpropiophenone (Sigma, 410896) in ethanol to form the functionalization solution. Gels were dehydrated with 70% ethanol for 5 minutes. The functionalization solution was added to the dehydrated gels followed by 10 minutes UV exposure. Gels were washed twice with 25mM HEPES for 5 minutes, followed by two 5-minute PBS washing steps. After removing the washing solution and blotting all liquid with paper, a protein solution consisting of 20 µg/ml either laminin-332 (Biolamina, LN332-0202) or laminin-511 (Biolamina, LN511-0202) with 30 µg/ml collagen IV (Sigma-Aldrich, M7027-100G) diluted in PBS++ (Gibco, 14040-091) was added as a bubble and incubated overnight.

Culture medium – A specific medium was prepared to accommodate the needs of the HiPSC-derived RPE cells. Medium was prepared with MEM alpha (ThermoFisher, 12571-063) with glutamax (Gibco, 35050-038), KnockOut serum (ThermoFisher, 10828-028), N-2 supplement (ThermoFisher, 17502-048), hydrocortisone (Sigma, H6909), taurine (Sigma, T0625), 1:1000 triiodo-L-thyronine (T₃) (Sigma, T5516), and gentamicin (ThermoFisher, 15750-060) (Sup. 1). After adding all components, the medium was filtered (Merck, SLGP033RB) to remove potential contaminations.

Cell seeding – Before seeding, dental glue rings were made using a 4 mm biopsy punch and sterilized for 40 minutes on the top, bottom, and side. Crosslinked hydrogels were sterilized under UV for 45 minutes in a PBS/gentamycin solution. After sterilization, the dental glue rings were placed around the gel. HiPSC-derived RPE cells (FUJIFILM Cellular Dynamics, R1102) were washed with EDTA/PBS and subsequently, for 30 minutes incubated at 37 °C with EDTA/PBS to remove calcium ions to weaken cell adhesion. After incubation, cells were loosened by resuspending and pipetted in the warm medium. TrypLE (Gibco, 12605-010) was added and incubated for 5 minutes at 37 °C to detach cells. After incubation, medium was used to wash the well and collect all cells into a medium vial. Collected cells were centrifuged at 1000g for 5 minutes. A sample was taken to be used for cell counting. Cells were seeded onto the hydrogel with a density of 50-75k cells per gel. Gels were left for 24 hours in the incubator (37 °C, 5% CO₂) to attach and subsequently, medium was added. The medium was changed twice weekly to ensure a constant growth environment.

Viral transduction – At day 10 after seeding, hydrogels were transduced with either an FKBP-casp8-mApple (VectorBuilder, VB230127-1043eaq) or GFP (VectorBuilder, VB010000-9394npt) containing AAV virus. A viral solution was made to pipet onto the hydrogels with a concentration of 2x10¹¹ FKBP-casp8-mApple viral particles/ml or equal GFP viral particles.

Apoptosis induction – At day 15, to initiate apoptosis, a 5 µM intermediate solution of AP20187 was prepared from 100mM stock (195514-80-8, Merck, Germany). A final solution of 100nM was made from the 5 µM intermediate stock and culture medium, which was subsequently pipetted onto the cells. The AP20187 solution was kept for 24 hours on the cells. After 24 hours, the medium was fully exchanged.

Nanoindentation – At day 17, nanoindentation was performed at Chiaro Nanoindentor device (Optics 11 Life) mounted on an inverted microscope with temperature-controlled atmosphere (Axio Observer 7, Zeis). A suitable probe was chosen with a tip radius of 11 µm and a stiffness of 0.017 N/m. The probe was allowed to acclimatize in the chamber at a controlled temperature (37°C). An optical calibration was performed by scanning the wavelength to determine the refractive index of the medium and subsequently, a geometrical factor was determined by probe indentation onto glass. A profile was set up with a matrix scan of 16 grid positions with 50 µm intervals. Displacement mode of 8000 nm indentation was selected during measurements. Dynamic mechanical analysis (DMA) mode was enabled, performing 1,2,4, and 10 Hz oscillations. Before performing the measurements, the medium

was exchanged. Measurements were analyzed by using Dataviewer v2 (Optics11 life, Netherlands). A Hertzian contact model was used in indentation mode to fit the 0-2500 nm portion of the indentation curve. The contact point was set within 30% of the maximum load and a Poisson's ratio of 0.5 was used for Young's modulus calculations. Fitted data were excluded if the correlation was lower than 0.95.

Immunostainings – Cells were fixated at room temperature by using a warm 2% paraformaldehyde (PFA) (Merck, 104005) solution for 8 minutes. Cells were permeabilized by using 0.3% triton in PBS solution. Aspecific bindings were blocked by using 1% BSA in PBS for 30 minutes. A primary antibody (sup. 2) was incubated overnight at 4 degrees. Cells were 3x washed with PBS before adding a secondary antibody (sup. 2) for 2 hours. Cells were again 3x washed with PBS before mounting with elvanol (Kuraray, Japan).

POS phagocytosis assay – Frozen POS were thawed, washed with medium, and centrifuged (2300g, 5 minutes). After resuspension, human Protein-S (Coachrom, pp012A), and MFG-E8 (R&D systems, 2767-MF-050) were added to aid POS phagocytosis. POS were seeded onto the cells to allow approximately 10-15 POS per RPE cell (1-1.5 million POS per gel). Cells were incubated for 4 hours, allowing internalization, and were subsequently 4x washed with warm PBS++. Cells were fixated with warm PFA 2% for 8 minutes. Aspecific bindings were blocked with 1% BSA for 1 hour, after which a primary anti-opsin antibody was added and incubated overnight. Cells were 3x washed with PBS and permeabilized with 0.3% triton in PBS. A secondary antibody, phalloidin, and DAPI were added and incubated for 2 hours. Cells were 3x washed with PBS and mounted with elvanol. For this analysis, a no-virus control was used instead of a GFP control to avoid overlap with the FITC-labelling of the POS. This condition was not transduced with AAV, but was subjected to the apoptosis induction with AP.

Imaging – Fluorescently labeled samples were imaged at Zeiss LSM 710 Confocal Microscope with Airyscan Super-resolution add-on or at Zeiss Imager.M2 with an apotome.2 add-on for optical sectioning. Z-slice thickness was equal at both microscopes at 0.5 μm per slice and imaging setting within an experimental set were uniform.

Extrusion event quantification – Cells were incubated for 3 hours with live staining SiR-actin (Spirochrome, SC001). Cells were put under a microscope under a controlled atmosphere (5% CO_2 , 37°C). The microscope was set up to take images in a 15-minute interval for at least 15 hours. To analyze the extrusion events, only the last 15 hours of the whole timelapse were taken. Images were aligned using the Template matching Fiji plugin, and a Gaussian blur of 2 μm was applied. After, a maximum intensity z-projection was applied. The amount of extrusion events was calculated by applying a threshold to generate masks. Mask particles of 10-350 μm^2 were included and counted.

Cell height quantification – To analyze cell height, actin staining was used and resliced to obtain an orthogonal view. Using the built-in rectangle Fiji tool, the height measurement was obtained.

Shape factor calculation – An actin z-stack was used as input for the analysis. First, a z-projection was made of the apical region. Cellpose (54) was used to segment pictures into regions of interest, encompassing each cell individually, and masks were created. Regions of interest were imported into Fiji and analyzed to determine the perimeter and area. The shape factor was determined by using the formula shape factor = perimeter/square root (area).

Statistical analysis – GraphPad Prism 10 (GraphPad, US) was used to visualize data and to determine significance at an alpha value of 0.05. Data were tested using a One-way ANOVA test, followed by Tukey's multiple comparisons. Standard errors displayed in figures use mean \pm standard deviation.

RESULTS

Physical and biochemical cues influence apoptosis efficiency – To mimic cell density reduction that RPE experiences in aging, large-scale apoptosis was induced in two-weeks old, polarized iPSC-derived RPE (Fig. 1A). This is possible thanks to cellular transduction with an AAV virus containing FKBP-casp8 on day 10 (Fig. 1B). AP20187 was added to activate the casp8 monomers on day 15. Due to the activated casp8 dimers coupled apoptosis induction, extrusion events of the monolayer could be visualized by live actin staining (Fig. 1C) and quantified using Fiji image analysis tools. Quantification of extrusion events shows as expected a significant difference in the number of extruded cells in the casp8 condition, compared to the GFP control condition (Fig. 1D). On soft substrates, biochemical cues influence extrusion events, which are more frequent on laminin-511 compared to laminin-332 coated

surfaces. Physical cues (i.e., stiffness) influence extrusion events only when the gels were coated with laminin-511, reducing the amount of extruding events with increased stiffness.

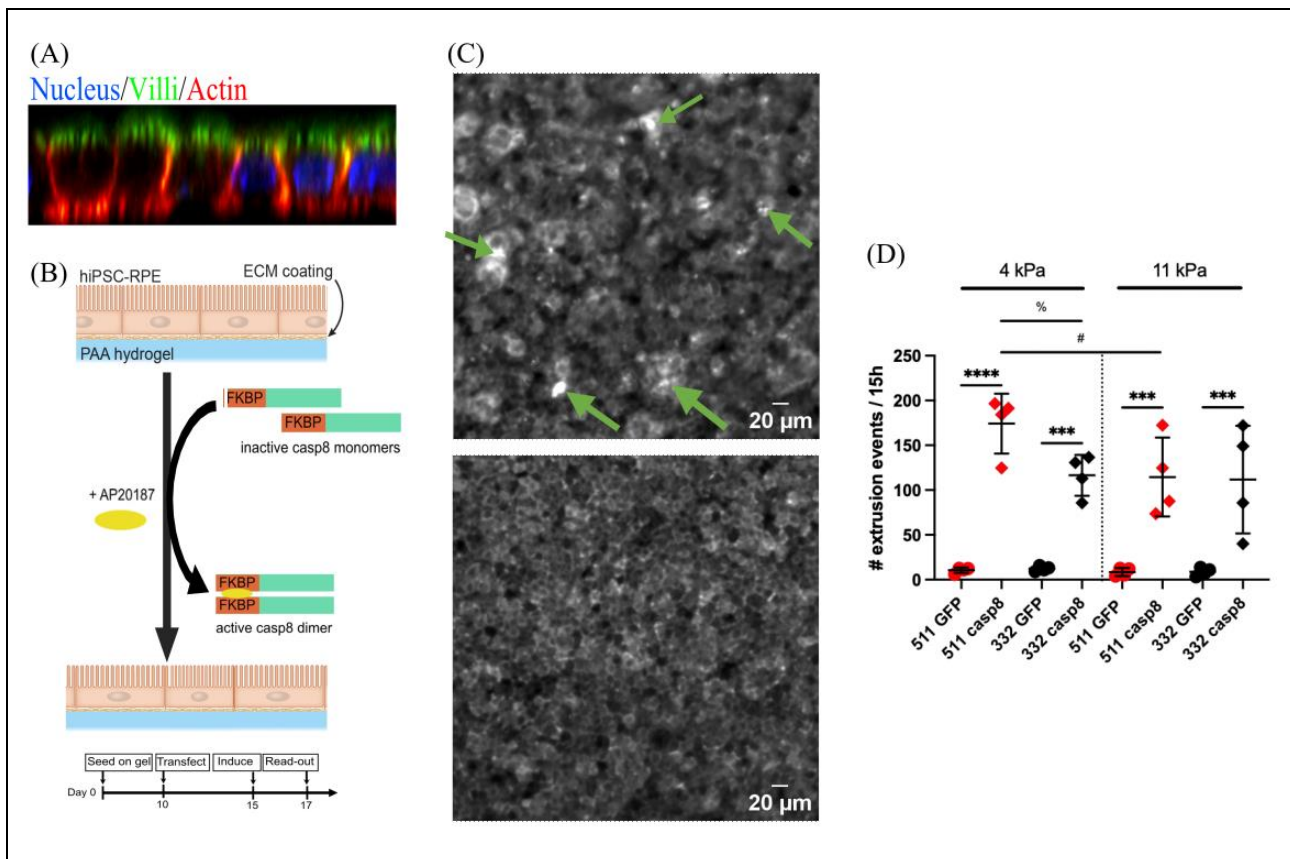


Fig. 1 – Physical cues influence apoptosis efficiency in laminin-511 coatings. (A) Orthogonal view of ezrin/actin/DAPI staining to indicate polarity of the model. (B) Schematic representation of the experimental model. (C) Z-projection of SiR-actin live-cell images of extrusion events during the last 15h recording. The upper picture represents an apoptosis induced condition, while the lower picture represents the GFP control condition. Green arrows indicate extrusion events. (D) Quantification of extrusion events during the last 15 hours of recording (n=4). Error bars are indicated as mean with standard deviation. ANOVA with multiple comparison was used to determine significance. 5% significance was applied. * indicates casp8 vs. GFP, # indicate 4 kPa vs. 11 kPa, and % indicates laminin-511 vs. laminin-332. * p<0.05, ** p<0.01, *** p<0.001, **** p<0.0001.

Structural adaptation after cell loss – The effect on cellular structure caused by the on-demand apoptosis model was assessed using several immunohistochemical stainings. Actin stainings show fibrous actin (F-actin) at the ECM-cell interface (Fig. 2A). Furthermore, F-actin was well represented near the lateral cellular membrane. More F-actin stress fibers were visible at casp8 conditions at stiffer substrates compared to the control. 4kPa conditions show no discernable difference. Next, junctions which are linked to the actin skeleton were evaluated. E-cadherin, a key component of adherens junctions, colocalizes with F-actin at the lateral cellular membranes (Fig. 2A). GFP conditions show fewer junctional E-cadherin colocalization compared to apoptosis-treated monolayers. After evaluating the actin cytoskeleton, we wanted to assess other cytoskeletal components. Keratin stainings show structural changes under the influence of apoptosis (Fig. 2B). Overall, the keratin network looks denser in apoptotic conditions than in control conditions, except for the 11kPa laminin-332 condition. Desmoplakin, a critical component of desmosomes, suggests increased clustering along cellular junctions in apoptosis-treated monolayers in soft substrates, while 11 kPa shows no notable changes (Fig. 2C). Lastly, cell height was quantified, showing an overall trend towards thinner cells in the model (Fig. 2D). Notably, physical cues influence cell height variance and baseline height, with control cells being taller on laminin-332 coated gels.

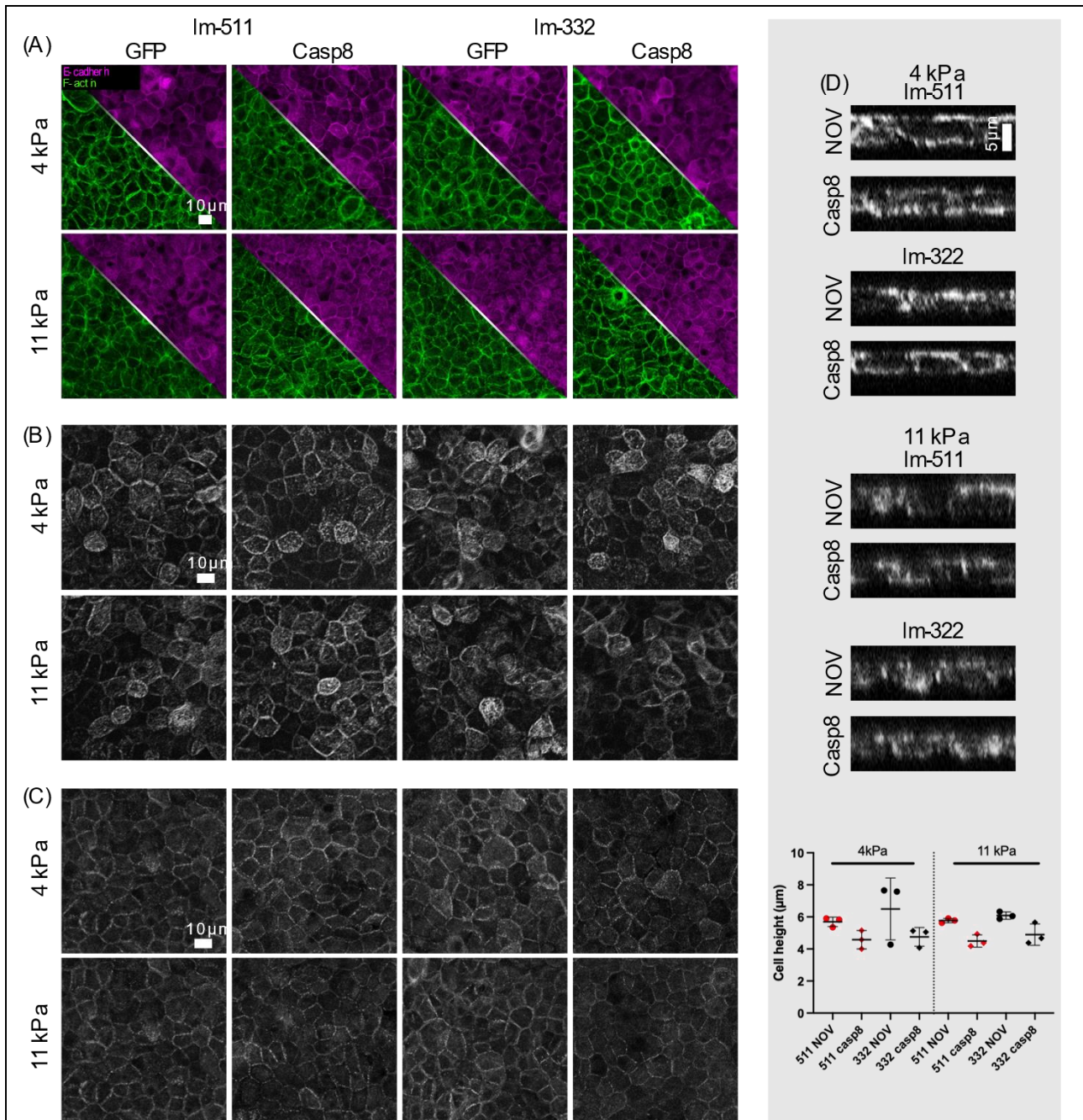


Fig. 2 – Apoptosis causes structural adaptation in cells. (A) Immunofluorescence staining of E-cadherin (adherens junction), and phalloidin (F-actin). (B) Immunofluorescence staining of keratin-8. (C) Immunofluorescence staining of desmoplakin. (D) Visualization of cell height with F-actin stainings in different conditions and quantification of cell height (n=3). Error bars are indicated as mean with standard deviation. ANOVA with multiple comparison was used to determine significance. 5% significance was applied. NOV = no virus.

Physical and biochemical cues influence the adaptation of cellular biomechanics – After determining the structural impact of our *in vitro* model, we determined the accompanying biomechanical changes. Shape factor quantification was performed to evaluate the mechanical state of the tissue based on cell morphology, with a higher shape factor indicating a more unjammed or fluid-like configuration (55). Overall, monolayers treated with large-scale apoptosis display a trend for lower shape factor, and, thus, a more jammed state, than the control (Fig. 3A). Jamming due to cell number reduction is significant on laminin-332 4kPa conditions. On laminin-511, physical cues affect shape factor adaptation after cell loss, with higher stiffness supporting a more unjammed state. Nanoindentation using an 11 µm spherical tip mounted on a flexible cantilever was performed to

evaluate stiffness, and viscoelastic properties (Fig. 3B). The effective Young's modulus shows cellular stiffening after cell number reduction, except for cells on softer hydrogels coated with laminin-511, where cells soften (Fig. 3C). Physical cues influence the baseline stiffness of cells, with softer substrates sustaining stiffer cells than stiffer substrates. Furthermore, biochemical cues determine the effects of the physical cues. Laminin-511 coatings cause a greater reaction to physical cues compared to laminin-332, cells on laminin-511 are significantly stiffer at 4 kPa than at 11 kPa. Furthermore, on 11 kPa and laminin-511 coating, cells significantly stiffen after uncompensated apoptosis. Storage modulus analysis reveals a trend towards higher elasticity after apoptosis on stiffer substrates, while soft conditions show comparable values (Fig. 3D). Loss modulus data indicate a trend of decreased viscosity after apoptosis in soft substrate conditions, while showing increased viscosity after cell loss in stiffer substrates, indicating an inverse effect depending on the physical cue (Fig. 3E). Furthermore, 4 kPa control conditions show a higher viscosity baseline compared to 11 kPa. Interestingly, both storage and loss modulus indicate that stiffer physical cues lead to greater viscosity and elasticity changes. Both the storage and loss modulus contribute to the Tan Delta (Fig. 3F), overall indicating a proportionally higher increase in elasticity, compared to viscosity after cell loss, indicating reduced dampening capacities. Softer substrates show a greater reduction while showing a higher variability than 11 kPa conditions. The laminin-511 control condition shows a reduced baseline compared to other control conditions. Further DMA results of 1,4, and 10 Hz storage-and-loss modulus, as well as Tan Delta show similar results and are therefore not included in this section (Sup. 3).

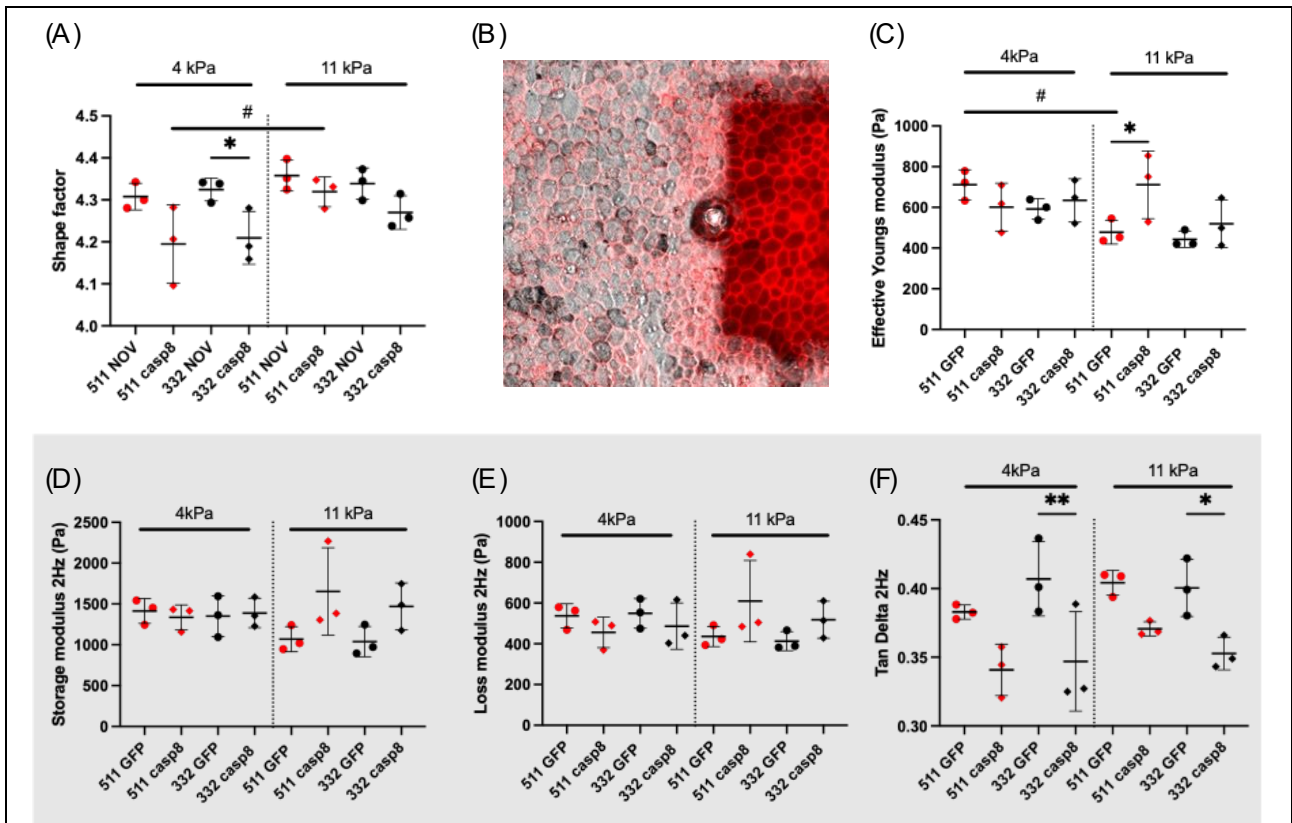


Fig. 3 – Physical and biochemical cues affect biomechanical adaptation. (A) Shape factor quantification (n=3). Lower values indicate a jammed state. (B) example of cantilever pressing down on cells. Cells are visualized by using a SiR-actin live staining (C) Effective Young's modulus quantification (n=3). Higher values indicate stiffer cells. (D) Storage modulus quantification (n=3). Higher values indicate higher elasticity. (E) Loss modulus quantification (n=3). Higher values indicate higher viscosity. (F) Tan Delta quantification (n=3). Higher values indicate a less elastic and more viscous sample. Error bars are indicated as mean with standard deviation. ANOVA with multiple comparison was used to determine significance. 5% significance was applied. * indicates casp8 vs. GFP, # indicates 4 kPa vs. 11 kPa. * p<0.05, ** p<0.01. NOV = no virus.

Structural remodeling affects cell-ECM adhesion and mechanosensitive signaling – To assess changes in mechanosensitive signaling, integrin $\beta 4$, Myocardin-related transcription factor A (MRTFA), and Phosphorylated myosin light chain (pMLC) were evaluated.

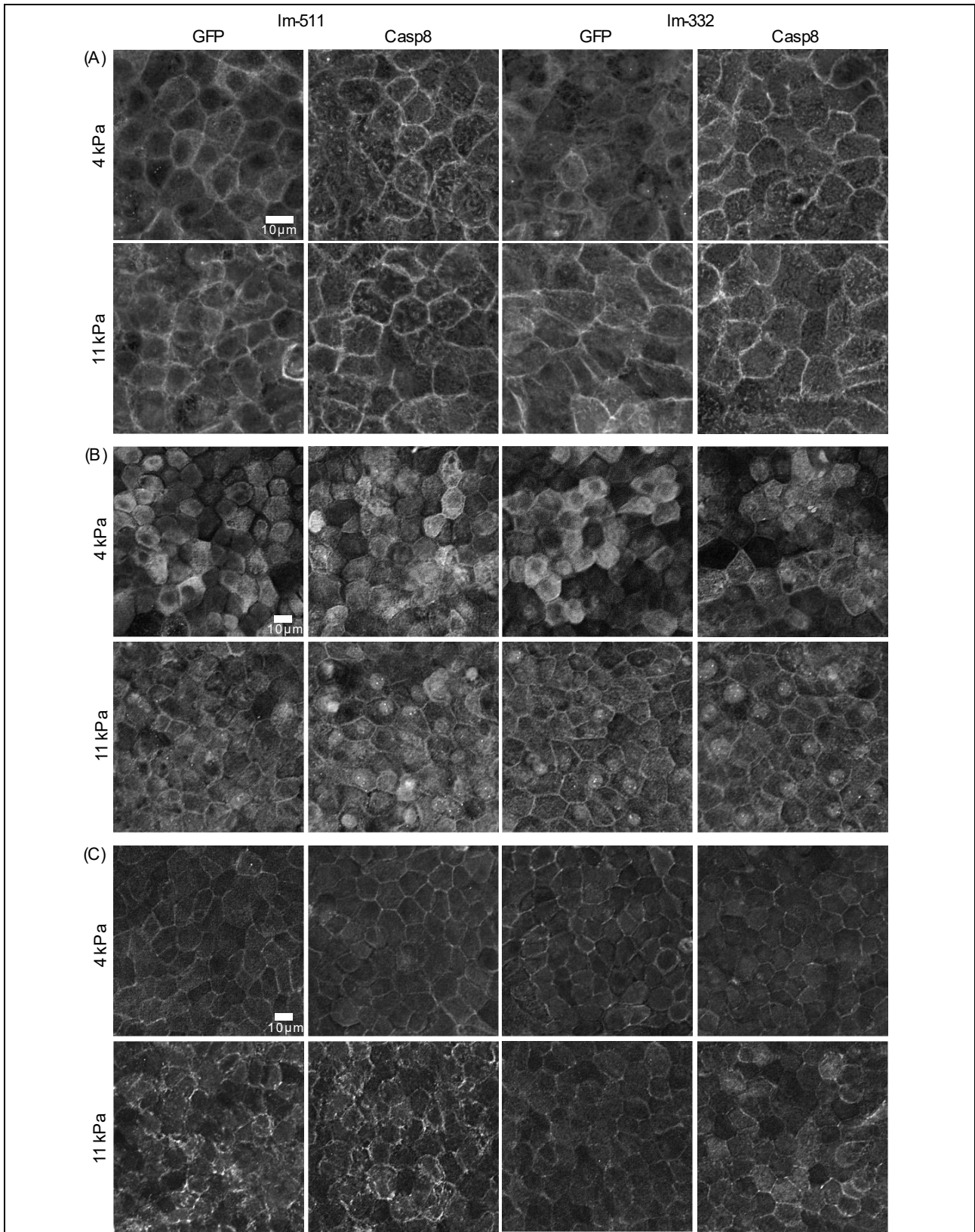


Fig. 4 – Molecular characterization of mechanobiological features. (A) Immunofluorescence staining of integrin $\beta 4$. (B) Immunofluorescence staining of MRTFA. (C) Immunofluorescence staining of pMLC. MRTFA = Myocardin Related Transcription Factor A, pMLC = phosphorylated myosin light chain.

Basal integrin $\beta 4$ stainings show a higher degree of signal density in casp8 conditions regardless of substrate stiffness, suggesting a rearrangement of integrin $\beta 4$ and different ECM adhesion (Fig. 4A). Furthermore, laminin-511 shows different clustering compared to laminin-332. MRTFA shows adaptability to physical cues by nuclear translocation in stiff substrates (Fig. 4B), while no translocation was present in 4kPa substrates. Furthermore, translocation is higher in the model. Higher degrees of nuclear translocation indicate a higher degree of communication between the cytoskeleton and the nucleus, therefore showing a higher degree of cytoskeletal dynamics. PMLC shows no discernible change in 4 kPa conditions (Fig. 4C). However, laminin-511 induced a distinct pMLC distribution in 11 kPa conditions. Furthermore, cell loss increased the expression of pMLC in laminin-332 coated soft hydrogels.

Structural remodeling reduces phagocytosis efficiency on soft laminin-511 coated hydrogels – As a readout of RPE functionality, POS internalization assay was performed (Fig. 5A). Non-phagocytized, external POS were stained with opsin before permeabilization to enable quantification, showing a significant reduction in efficiency at 4 kPa hydrogels coated with laminin-511 (Fig. B, C). An overall trend in reduction of POS phagocytosis efficiency was visible upon uncompensated apoptosis in all conditions. Monolayers on laminin-511 coated substrates experienced a greater overall reduction in phagocytosis efficiency upon cell loss compared to laminin-332 conditions. Furthermore, baseline phagocytosis efficiency was higher with stiffer substrates.

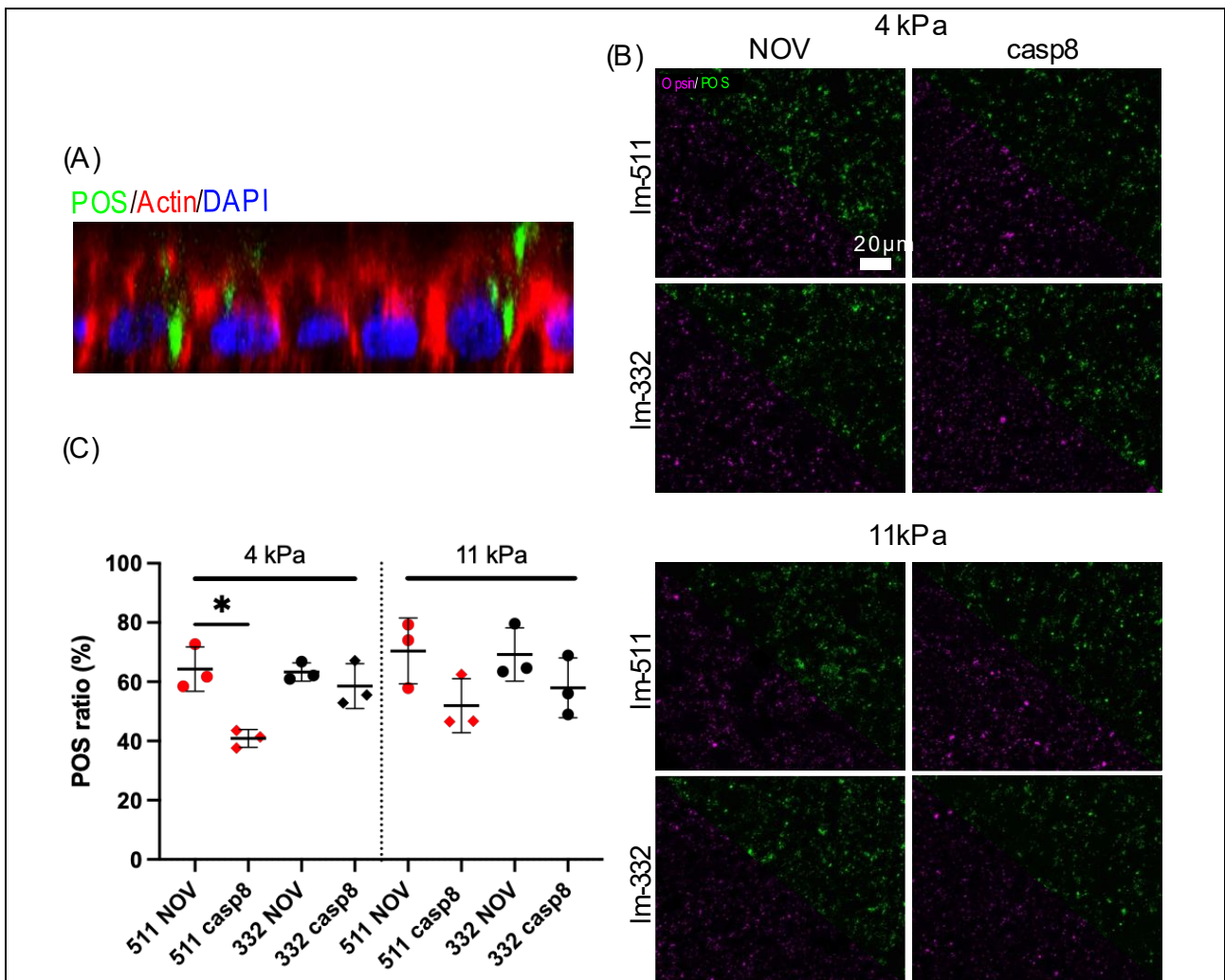
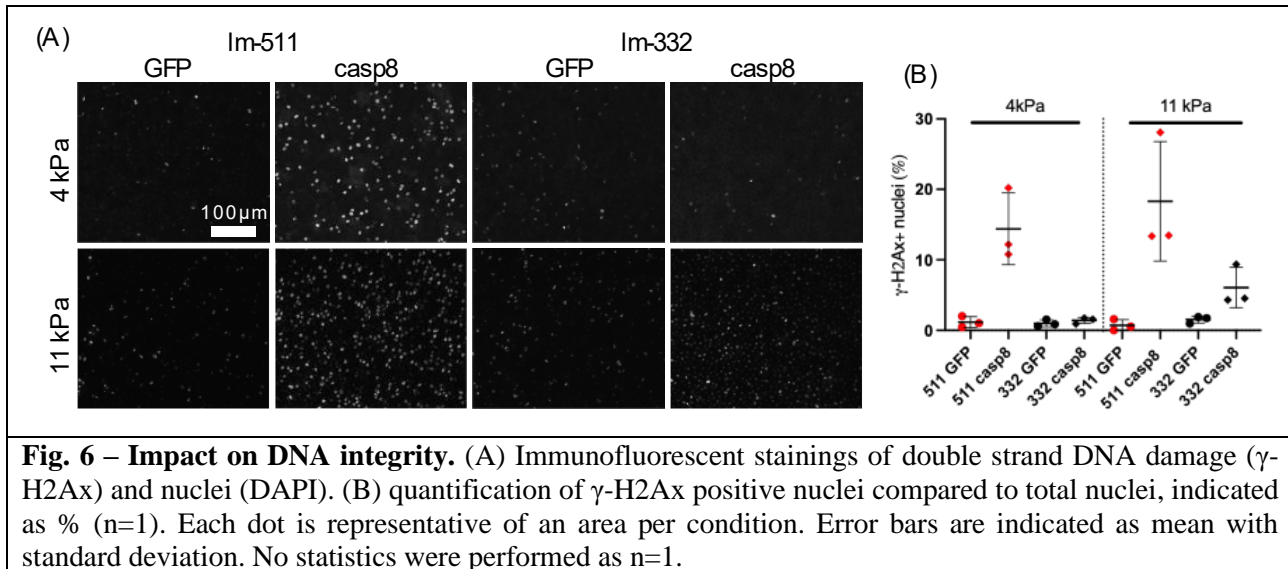


Fig. 5 – POS internalization analysis. (A) Overview figure of POS internalization assay. (B) Immunofluorescence staining of extracellular photoreceptors (opsin), intracellular photoreceptors (POS). (C) POS assay quantification of intracellular POS vs. extracellular POS (opsin) (n=3). Error bars are indicated as mean with standard deviation. ANOVA with multiple comparison was used to determine significance. 5% significance was applied. * indicates casp8 vs. NOV. * $p \leq 0.05$. POS = Photoreceptor outer segments, NOV = no virus.

Physical and biochemical cues influence double-strand breaks – To assess DNA damage, double-strand breaks (DSBs) were determined by staining for γ -H2Ax (Fig. 6A). Overall, RPE after uncompensated apoptosis show more DNA damage foci compared to control, except for 4kPa laminin-332 conditions (Fig. 6A, B). Both physical and biochemical cues influence DSBs. Laminin-511 shows increased DSBs in both soft and stiff substrates. However, physical cues show a DSB inducing trend, both elevating DSB occurrence in laminin-511 conditions and inducing DSBs in stiff substrates coated with laminin-332.



DISCUSSION

Model for researching aged retinal tissue – During this research, we provided a suitable model for studying the mechanical aspects of aging in RPE tissue, and which role ECM proteins offer in this process (Fig. 1). Our *in vitro* model replicates multiple characteristics of *in vivo* aging such as increased apoptosis (56), a trend for decreasing cell height (6), and reduced phagocytosis efficiency (57), while retaining correct polarity. In casp8 conditions, higher rates of cell loss could lead to a reduction of the total amount of cells, requiring the remaining cells to fill in the gaps to complete the monolayer, leading to thinning of cells.

Physical and biochemical cues drive biomechanical adaptations of aged RPE – Overall, observations from our model of RPE subjected to cell loss concurred with data in aged *in vivo* RPE tissue, which described aged cells as larger and more irregular (Fig. 3) (22). Cell loss in the model provides overall the biggest influence on cell shape, stiffness, elasticity, and viscosity, as opposed to ECM cues which have more subtle modulatory implications. Physical ECM cues affected the biomechanical and morphological adaptation to cell loss. Interestingly, softer substrates amplified the effect on the shape factor and viscoelastic properties, while stiffer substrates magnified the effect of cell loss on stiffness. First, we evaluated the shape factor, which shows a reduction after cell loss, indicating a more jammed state. Classically, a jammed state indicates tissue homeostasis, rigidity, and mechanical stability while an unjammed state indicates a more dynamic system with mechanical fluidity and plasticity which has high adaptability to the environment (23, 25). Following this line of thought, cell loss may increase the mechanical stability of the system in an effort to counterbalance the mechanical stress of cell loss. Desmoplakin stainings show presumably increased desmosome formation, increasing mechanical stability and reinforcing the cell-cell contacts (Fig. 2). Desmosome-keratin scaffold contributes to mechanical stability of stressed cells and may be involved in mechanosensory capacity (58, 59). Furthermore, 4 kPa substrates show higher variability and a greater reduction in shape factor, compared to their stiffer counterparts. This could be due to the more dynamic nature of both the cytoskeleton and cell-cell/cell-ECM adhesion on softer substrates, further explaining the baseline reduction of the shape factor. The stiffness of cells is primarily influenced by laminin-511, whereas laminin-332 provides a protective effect. This indicates that laminin-511 allows for greater cellular effects in response to physical substrate alterations. Previous research indicates that laminin-511 is

central to mechanotransduction in endothelial cells and influences stiffness (60). We show that the same concept might apply to the RPE as well. This could be explained by higher traction forces and higher contractility which laminin-511 promotes (53), probably causing cells to maintain a more dynamic actin cytoskeleton and leading to increased actin turnover. Meanwhile, viscoelastic properties seem to be influenced to a higher degree by biochemical cues instead of physical cues. This may stem from the dominant cytoskeleton component that specific laminin isoforms engage. It is known that keratin filaments, which are probably better engaged on hemidesmosome-forming laminin-332 substrates, can elongate and retain their stiffness (61). Obtained results might indicate elongation of the keratin cytoskeleton, which might affect its dampening ability, while still being able to contribute to cellular stiffness. Further results indicate that laminin-332 loses its protective effect and cells become more elastic and less viscous, showing reduced dampening abilities. This might indicate that laminin-332 is primarily influencing viscoelastic properties. Laminin-332 seems to be less affected by substrate stiffness changes compared to laminin-511, indicating that laminin-332 has a protective effect towards substrate stiffness fluctuations. Increased mechanical stability of 4 kPa conditions can further be seen in terms of Young's modulus measurements, indicating fewer fluctuations compared to 11 kPa conditions. Aging causes increased stiffness of the Bruch's membrane in the *in vivo* eye (3, 22), suggesting that higher stiffness may be less permissive for healthy functioning. This agrees with our observation that softer substrates induce less pronounced mechanical fluctuation as an adaptation to cell loss. Since we observed a stiffening response only on laminin-511 at 11 kPa, the laminin-511/laminin-332 composition within different retinal areas, could therefore affect the biomechanical changes in the aging RPE. Increased substrate stiffness favors reinforced cell-substrate adhesions (62). Here we provide further proof of increased stiffness contributing to an unjammed collective cellular state. We expand this concept by further evaluating biochemical cues. At higher substrate stiffness, laminin-511 seems to have a magnifying effect on promoting a more fluid-like, less jammed state by providing stronger cell-substrate adhesion. This is in line with previous work of the group, showing that laminin-511 promote higher traction forces than laminin-332 (53). Mechanical stability requires increased cell-substrate adhesion (62), which can be seen by integrin $\beta 4$ (Fig. 4), which together with integrin $\alpha 6$ usually forms hemidesmosome linking the cellular keratin network to the substrate (63). Upon cell loss, RPE on both laminin conditions show increased restructuring of $\beta 4$ signal, signifying a higher clustering/recruitment or increased heterogeneity of adhesion. The effect is highly pronounced on laminin-511. One theory explaining a difference in $\beta 4$ signal is the molecular clutch mechanisms, which can be tuned by substrate stiffness (50). Therefore, increasing substrate stiffness leads to increased traction forces generated by cells. Increased substrate stiffness and cell traction force are accompanied by additional focal adhesions and integrin clustering to maintain high force transmission (50, 52). Integrin $\beta 4$ clustering can be seen on stiff gels in both laminin-511 and laminin-332 after cell loss (Fig. 4). Further insights could be provided by looking at $\beta 1$ based adhesion, which links the more dynamic actin cytoskeleton. All factors combined explain why 4 kPa conditions generally show less effects of changing physical cues, and why biochemical cues can be amplifying or protective of the effects of substrate stiffness. Due to molecular clutch mechanisms and its mechanical stability provided by jammed states, 4 kPa conditions show less effect of changing physical cues. This effect can further be seen by looking at MRTFA translocation in the nucleus (Fig. 4B), which indicates mechanotransduction (64). Here, translocation in the nuclei is only present in 11 kPa conditions and more nuclear translocation is seen in laminin-511 nuclei compared to laminin-332. MRTFA translocation controls the expression of structural and regulatory components of the actin cytoskeleton, which control actin dynamics (64). We see that increasing substrate stiffness causes increased translocation, while laminin-511 and cell loss in stiffer substrates aggravate this translocation, indicating increased actin dynamics in these conditions.

POS internalization in aging – results show a significant reduction of POS internalization in 4 kPa coated with laminin-511 (Fig. 5), which is in agreement with lower POS internalization efficiency seen in aged RPE *in vivo* (57, 65). However, obtained results could have multiple interpretations. Either the outer segments are less internalized, or internalized POS are faster degraded. However, based on characterization indicating a trend of decreased Tan Delta and shape factors, a possible change in mechanics, and thus in contractility is likely. Current research proves that elevated contractility levels inhibit POS internalization (53). We see elevated pMLC expression (Fig. 4C) mainly in 11 kPa caspase conditions, which indicates higher contractility. Baseline pMLC expression is increased in laminin-511

11kPa conditions. However, we show a significant decrease in phagocytosis efficiency in 4kPa, laminin-511 coated conditions with cell loss and see only a decreasing trend in 11 kPa conditions. Contractility could contribute to the decrease in internalization rate at high substrate stiffnesses, while viscoelastic properties influence softer substrate conditions more. Furthermore, biochemical cues influence function where laminin-332 again shows a protective effect.

Impact on DNA integrity – Both physical and biochemical cues influence double-strand DNA damage. Overall, stiffer substrates promote more DSBs, which can be a result of higher capability for force generation on stiffer substrates (66) and, thus, a higher ‘stretching’ of the tissue by cell loss. In softer substrate laminin-332 conditions, no DSB can be found, while in stiffer substrates a limited amount can be found. Additionally, biochemical cues affect DSBs. We already stipulated that laminin-332 has a protective effect against substrate stiffnesses, which is further supported here. Laminin-511 coatings show high DSB percentages, while laminin-332 conditions show little or none. We showed that laminin-511 seems to be more responsive towards substrate stiffness, which could lead to increased nuclear stress and DNA damage. However, these results are not fully conclusive as only one experiment has been conducted and more should follow to make a grounded final statement on DSBs.

Limitations – Our research model is based on one-time, large-scale casp-8-mediated apoptotic induction, which is not equal to continuous cell death due to aging. The readout time is 24 hours after the apoptosis, meaning cells have to respond to acute cell loss instead of chronic, leaving less time to adapt. Our model uses hiPSC-derived RPE, which is very young and might show different behavior compared to old cells. The ECM coating consists of laminins and collagen type IV, potentially affecting results, and making it less clear if this is a pure laminin-caused effect. Lastly, several evaluations of structural, as well as functional readouts have not been quantified, leaving room for subjective interpretations. Therefore, the impact of cellular reduction has to be further characterized by Western blots to provide more objective interpretations of potential changes.

Implications - These results fill the knowledge gap on the role of chemical and physical cues on RPE biomechanics and its subsequent implications on retinal function in a model of age-mimicking remodeling. Furthermore, little information on the biomechanics of post-mitotic tissues is known, thereby expanding the knowledge of crucial mechanisms that could have potential use in regenerative medicine and RPE transplantation. For example, ECM composition is known to play an important role in pancreatic islet function and survival after transplantation (67). Here, ECM restoring strategies have been shown to improve transplantation outcome (67). Therefore, understanding how the ECM influences the RPE could help with RPE transplantation in diseases such as age-related macular degeneration (AMD) and Stargardt’s macular dystrophy, where trials have been conducted (68).

Future outlook – Multiple avenues can be pursued to further investigate this topic. Laminin concentrations can be changed to address the changes in laminin proteins across the retina *in vivo*. Further insights into the aging process of our model can be gathered by further looking into DNA damage, mitochondria dysfunction, cellular senescence, and involved molecular pathways. Integrin $\beta 4$ quantification could potentially be done in the future by Gray-level Co-occurrence Matrix (GLCM) to better understand integrin restructuring. As mentioned, other integrins, such as $\beta 1$, could further explain observed changes and further characterize the model. Structural remodeling of the model has to be further characterized using western blots to better interpret the biomechanical adaptation and the root cause. Desmoplakin stainings can be conducted with desmosome co-localizing proteins to confirm desmosome locations.

CONCLUSION

Our *in vitro* aging model is characterized by cell loss, thinning of cells, and impaired phagocytosis efficiency, which are hallmarks of RPE aging seen in the elderly. This model is a valuable tool to further evaluate and characterize aging RPE, while not relying on fixated human tissue samples or animals. Furthermore, this model underscores further the significance of both physical and biochemical cues to the biomechanical properties of the cell. While acknowledging the limitations of the model such as acute cell loss compared to chronic, the inherent nature of hiPSCs, the versatility of the model stands out as being highly tunable, providing a suitable platform to investigate different ECM stiffnesses, and protein compositions to evaluate structural, biomechanical, and functional changes. Results reveal that biomechanical adaptations caused by cell loss are modulated by substrate stiffness and ECM protein

composition. Soft substrates amplify the effect of cell loss, morphology, and viscoelastic properties, while stiff substrates mainly affect stiffness, contractility, and mechanotransduction pathways. Different laminin isoforms show distinct responsiveness to physical cues. The discussion reveals how certain biomechanical adaptations can be explained by mechanisms involving the molecular clutch, integrin clustering, or cytoskeletal dynamics in response to either physical or biochemical cues. Furthermore, we shed light on its functional implications such as POS internalization and DNA integrity. In conclusion, the findings of this study elaborate on the mechanical aspects of the RPE aging process using our novel model to simulate cell loss in the RPE during the natural aging process. Our findings show biomechanical and functional adaptations in our model, driven by the interplay between physical and biochemical cues. These insights can be used to potentially improve transplantation of the RPE or other tissues by controlling ECM influences.

REFERENCES

1. Yang S, Zhou J, Li D. Functions and Diseases of the Retinal Pigment Epithelium. *Front Pharmacol.* 2021;12:727870.
2. Boulton M, Dayhaw-Barker P. The role of the retinal pigment epithelium: topographical variation and ageing changes. *Eye (Lond).* 2001;15(Pt 3):384-9.
3. Hammadi S, Tzoumas N, Ferrara M, Meschede IP, Lo K, Harris C, et al. Bruch's Membrane: A Key Consideration with Complement-Based Therapies for Age-Related Macular Degeneration. *J Clin Med.* 2023;12(8).
4. Gao H, Hollyfield JG. Aging of the human retina. Differential loss of neurons and retinal pigment epithelial cells. *Invest Ophthalmol Vis Sci.* 1992;33(1):1-17.
5. Panda-Jonas S, Jonas JB, Jakobczyk-Zmija M. Retinal pigment epithelial cell count, distribution, and correlations in normal human eyes. *Am J Ophthalmol.* 1996;121(2):181-9.
6. Katz ML, Robison WG. Age-related changes in the retinal pigment epithelium of pigmented rats. *Experimental Eye Research.* 1984;38(2):137-51.
7. Salem MA. Structure and function of the retinal pigment epithelium, photoreceptors and cornea in the eye of *Sardinella aurita* (Clupeidae, Teleostei). *The Journal of Basic & Applied Zoology.* 2016;75:1-12.
8. Kocaoglu OP, Liu Z, Zhang F, Kurokawa K, Jonnal RS, Miller DT. Photoreceptor disc shedding in the living human eye. *Biomed Opt Express.* 2016;7(11):4554-68.
9. Bonilha VL. Age and disease-related structural changes in the retinal pigment epithelium. *Clin Ophthalmol.* 2008;2(2):413-24.
10. Marmorstein AD. The polarity of the retinal pigment epithelium. *Traffic.* 2001;2(12):867-72.
11. Stricker J, Falzone T, Gardel ML. Mechanics of the F-actin cytoskeleton. *Journal of Biomechanics.* 2010;43(1):9-14.
12. Pollard TD, Cooper JA. Actin, a Central Player in Cell Shape and Movement. *Science.* 2009;326(5957):1208-12.
13. Fletcher DA, Mullins RD. Cell mechanics and the cytoskeleton. *Nature.* 2010;463(7280):485-92.
14. Bonilha VL. Retinal pigment epithelium (RPE) cytoskeleton in vivo and in vitro. *Experimental Eye Research.* 2014;126:38-45.
15. Tarau IS, Berlin A, Curcio CA, Ach T. The Cytoskeleton of the Retinal Pigment Epithelium: from Normal Aging to Age-Related Macular Degeneration. *Int J Mol Sci.* 2019;20(14).
16. Miyoshi J, Takai Y. Molecular perspective on tight-junction assembly and epithelial polarity. *Adv Drug Deliv Rev.* 2005;57(6):815-55.
17. Kowalczyk AP, Green KJ. Structure, function, and regulation of desmosomes. *Prog Mol Biol Transl Sci.* 2013;116:95-118.
18. Hartsock A, Nelson WJ. Adherens and tight junctions: structure, function and connections to the actin cytoskeleton. *Biochim Biophys Acta.* 2008;1778(3):660-9.
19. Tsukita S. Tight Junctions. In: Lennarz WJ, Lane MD, editors. *Encyclopedia of Biological Chemistry (Second Edition)*. Waltham: Academic Press; 2013. p. 392-5.
20. Gumbiner BM. Regulation of cadherin-mediated adhesion in morphogenesis. *Nat Rev Mol Cell Biol.* 2005;6(8):622-34.
21. Ladoux B, Nelson WJ, Yan J, Mège RM. The mechanotransduction machinery at work at adherens junctions. *Integr Biol (Camb).* 2015;7(10):1109-19.
22. von der Emde L, Vaisband M, Hasenauer J, Bourauel L, Bermond K, Saßmannshausen M, et al. Histologic Cell Shape Descriptors for the Retinal Pigment Epithelium in Age-Related Macular Degeneration: A Comparison to Unaffected Eyes. *Transl Vis Sci Technol.* 2022;11(8):19.

23. Atia L, Fredberg JJ, Gov NS, Pegoraro AF. Are cell jamming and unjamming essential in tissue development? *Cells Dev.* 2021;168:203727.
24. Lawson-Keister E, Manning ML. Jamming and arrest of cell motion in biological tissues. *Current Opinion in Cell Biology.* 2021;72:146-55.
25. Cai G, Nguyen A, Bashirzadeh Y, Lin SS, Bi D, Liu AP. Compressive stress drives adhesion-dependent unjamming transitions in breast cancer cell migration. *Front Cell Dev Biol.* 2022;10:933042.
26. Booij JC, Baas DC, Beisekeeva J, Gorgels TG, Bergen AA. The dynamic nature of Bruch's membrane. *Prog Retin Eye Res.* 2010;29(1):1-18.
27. Johnson PT, Lewis GP, Talaga KC, Brown MN, Kappel PJ, Fisher SK, et al. Drusen-Associated Degeneration in the Retina. *Investigative Ophthalmology & Visual Science.* 2003;44(10):4481-8.
28. Huang JD, Presley JB, Chimento MF, Curcio CA, Johnson M. Age-related changes in human macular Bruch's membrane as seen by quick-freeze/deep-etch. *Exp Eye Res.* 2007;85(2):202-18.
29. Ugarte M, Hussain AA, Marshall J. An experimental study of the elastic properties of the human Bruch's membrane-choroid complex: relevance to ageing. *Br J Ophthalmol.* 2006;90(5):621-6.
30. Elnér SG, Elnér VM. The integrin superfamily and the eye. *Invest Ophthalmol Vis Sci.* 1996;37(5):696-701.
31. Yang X, Chung JY, Rai U, Esumi N. Cadherins in the retinal pigment epithelium (RPE) revisited: P-cadherin is the highly dominant cadherin expressed in human and mouse RPE in vivo. *PLoS One.* 2018;13(1):e0191279.
32. Hynes RO. Integrins: Bidirectional, Allosteric Signaling Machines. *Cell.* 2002;110(6):673-87.
33. Afshari FT, Fawcett JW. Improving RPE adhesion to Bruch's membrane. *Eye.* 2009;23(10):1890-3.
34. Humphries JD, Byron A, Humphries MJ. Integrin ligands at a glance. *J Cell Sci.* 2006;119(Pt 19):3901-3.
35. Arimori T, Miyazaki N, Mihara E, Takizawa M, Taniguchi Y, Cabañas C, et al. Structural mechanism of laminin recognition by integrin. *Nature Communications.* 2021;12(1):4012.
36. Aumailley M. The laminin family. *Cell Adh Migr.* 2013;7(1):48-55.
37. Aumailley M, Bruckner-Tuderman L, Carter WG, Deutzmann R, Edgar D, Ekblom P, et al. A simplified laminin nomenclature. *Matrix Biol.* 2005;24(5):326-32.
38. Nishiuchi R, Takagi J, Hayashi M, Ido H, Yagi Y, Sanzen N, et al. Ligand-binding specificities of laminin-binding integrins: A comprehensive survey of laminin-integrin interactions using recombinant $\alpha 3\beta 1$, $\alpha 6\beta 1$, $\alpha 7\beta 1$ and $\alpha 6\beta 4$ integrins. *Matrix Biology.* 2006;25(3):189-97.
39. Rousselle P, Beck K. Laminin 332 processing impacts cellular behavior. *Cell Adh Migr.* 2013;7(1):122-34.
40. Miner JH, Patton BL, Lentz SI, Gilbert DJ, Snider WD, Jenkins NA, et al. The laminin alpha chains: expression, developmental transitions, and chromosomal locations of alpha1-5, identification of heterotrimeric laminins 8-11, and cloning of a novel alpha3 isoform. *J Cell Biol.* 1997;137(3):685-701.
41. Burridge K, Chrzanoska-Wodnicka M. Focal adhesions, contractility, and signaling. *Annu Rev Cell Dev Biol.* 1996;12:463-518.
42. Janmey PA, Fletcher DA, Reinhart-King CA. Stiffness Sensing by Cells. *Physiol Rev.* 2020;100(2):695-724.

43. Kennedy KM, Bhaw-Luximon A, Jhurry D. Cell-matrix mechanical interaction in electrospun polymeric scaffolds for tissue engineering: Implications for scaffold design and performance. *Acta Biomater.* 2017;50:41-55.
44. van der Flier A, Sonnenberg A. Function and interactions of integrins. *Cell Tissue Res.* 2001;305(3):285-98.
45. Harris AR, Jreij P, Fletcher DA. Mechanotransduction by the Actin Cytoskeleton: Converting Mechanical Stimuli into Biochemical Signals. *Annual Review of Biophysics.* 2018;47(Volume 47, 2018):617-31.
46. Luo Q, Kuang D, Zhang B, Song G. Cell stiffness determined by atomic force microscopy and its correlation with cell motility. *Biochimica et Biophysica Acta (BBA) - General Subjects.* 2016;1860(9):1953-60.
47. Hao J, Zhang Y, Jing D, Shen Y, Tang G, Huang S, et al. Mechanobiology of mesenchymal stem cells: Perspective into mechanical induction of MSC fate. *Acta Biomater.* 2015;20:1-9.
48. Engler AJ, Richert L, Wong JY, Picart C, Discher DE. Surface probe measurements of the elasticity of sectioned tissue, thin gels and polyelectrolyte multilayer films : correlations between substrate stiffness and cell adhesion. *Surface Science.* 2004;570:142-54.
49. Mierke CT. Viscoelasticity, Like Forces, Plays a Role in Mechanotransduction. *Frontiers in Cell and Developmental Biology.* 2022;10.
50. Elosegui-Artola A, Trepas X, Roca-Cusachs P. Control of Mechanotransduction by Molecular Clutch Dynamics. *Trends in Cell Biology.* 2018;28(5):356-67.
51. Swaminathan V, Waterman CM. The molecular clutch model for mechanotransduction evolves. *Nat Cell Biol.* 2016;18(5):459-61.
52. Paszek MJ, Boettiger D, Weaver VM, Hammer DA. Integrin clustering is driven by mechanical resistance from the glycocalyx and the substrate. *PLoS Comput Biol.* 2009;5(12):e1000604.
53. Kozyrina AN, Piskova T, Semeraro F, Doolaar IC, Prapty T, Haraszti T, et al. Laminin-defined Mechanical Status Modulates Retinal Pigment Epithelium Functionality. *bioRxiv.* 2024:2023.02.24.529913.
54. Stringer C, Wang T, Michaelos M, Pachitariu M. Cellpose: a generalist algorithm for cellular segmentation. *Nature Methods.* 2021;18(1):100-6.
55. Park JA, Kim JH, Bi D, Mitchel JA, Qazvini NT, Tantisira K, et al. Unjamming and cell shape in the asthmatic airway epithelium. *Nat Mater.* 2015;14(10):1040-8.
56. Del Priore LV, Kuo Y-H, Tezel TH. Age-Related Changes in Human RPE Cell Density and Apoptosis Proportion In Situ. *Investigative Ophthalmology & Visual Science.* 2002;43(10):3312-8.
57. Inana G, Murat C, An W, Yao X, Harris IR, Cao J. RPE phagocytic function declines in age-related macular degeneration and is rescued by human umbilical tissue derived cells. *Journal of Translational Medicine.* 2018;16(1):63.
58. Hatzfeld M, Keil R, Magin TM. Desmosomes and Intermediate Filaments: Their Consequences for Tissue Mechanics. *Cold Spring Harb Perspect Biol.* 2017;9(6).
59. Elbalasy I, Mollenkopf P, Tutmarc C, Herrmann H, Schnauß J. Keratins determine network stress responsiveness in reconstituted actin–keratin filament systems. *Soft Matter.* 2021;17(14):3954-62.
60. Di Russo J, Luik AL, Yousif L, Budny S, Oberleithner H, Hofschröder V, et al. Endothelial basement membrane laminin 511 is essential for shear stress response. *Embo j.* 2017;36(2):183-201.
61. Lorenz C, Forsting J, Style RW, Klumpp S, Köster S. Keratin filament mechanics and energy dissipation are determined by metal-like plasticity. *Matter.* 2023;6(6):2019-33.

62. Vazquez K, Saraswathibhatla A, Notbohm J. Effect of substrate stiffness on friction in collective cell migration. *Scientific Reports*. 2022;12(1):2474.
63. Jones JC, Kurpakus MA, Cooper HM, Quaranta V. A function for the integrin alpha 6 beta 4 in the hemidesmosome. *Cell Regul*. 1991;2(6):427-38.
64. Olson EN, Nordheim A. Linking actin dynamics and gene transcription to drive cellular motile functions. *Nature Reviews Molecular Cell Biology*. 2010;11(5):353-65.
65. Piskova T, Kozyrina AN, Di Russo J. Mechanobiological implications of age-related remodelling in the outer retina. *Biomaterials Advances*. 2023;147:213343.
66. Califano JP, Reinhart-King CA. Substrate Stiffness and Cell Area Predict Cellular Traction Stresses in Single Cells and Cells in Contact. *Cell Mol Bioeng*. 2010;3(1):68-75.
67. Smink AM, de Vos P. Therapeutic Strategies for Modulating the Extracellular Matrix to Improve Pancreatic Islet Function and Survival After Transplantation. *Current Diabetes Reports*. 2018;18(7):39.
68. Zartasht Khan A, Utheim TP, Eidet JR. Retinal Pigment Epithelium Transplantation: Past, Present, and Future. *J Ophthalmic Vis Res*. 2022;17(4):574-80.

Acknowledgements – JS is grateful for the opportunity to perform his master’s thesis at the REMeD lab of JdR. JS is thankful for the expert day-to-day supervision TP provided during the internship. JS is grateful for the mentoring JdR provided during the internship.

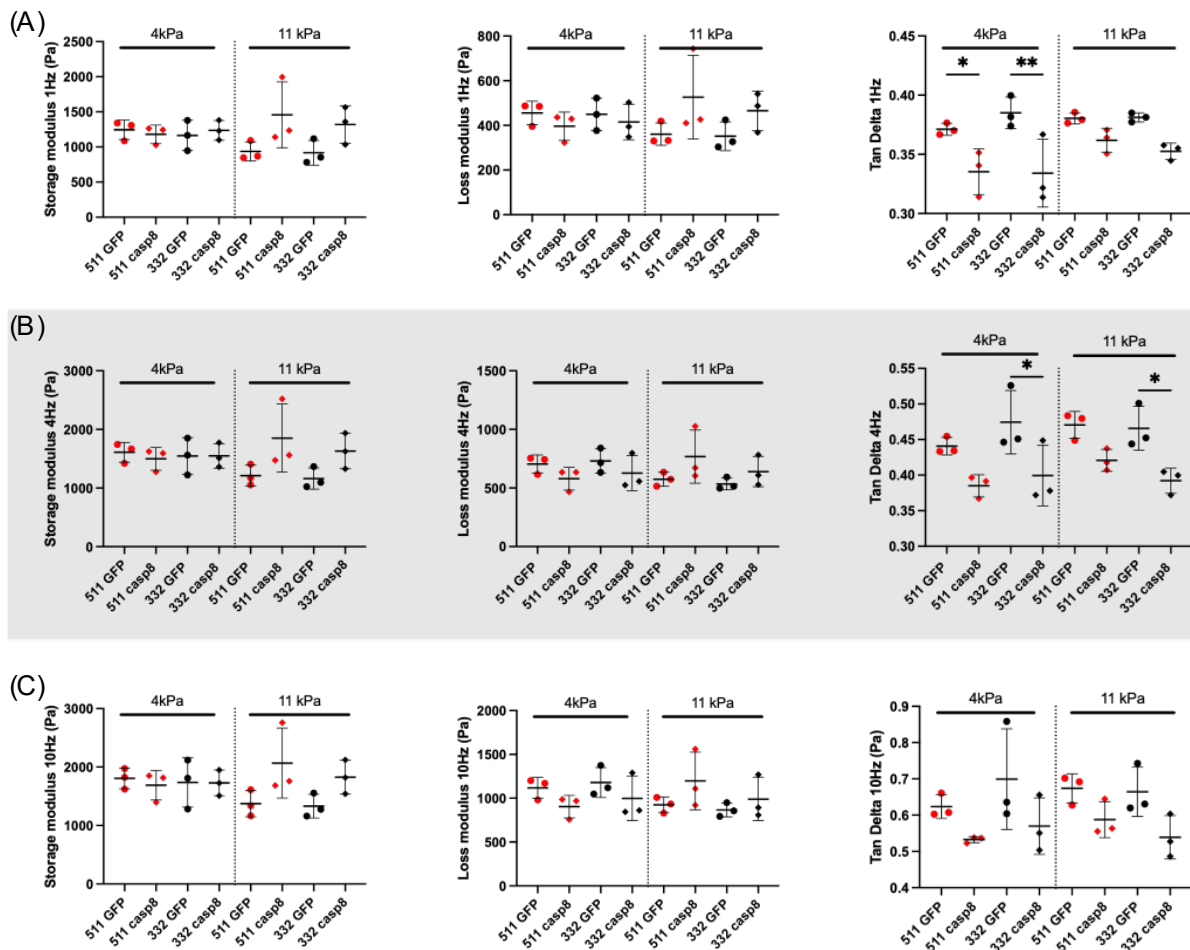
Author contributions – JdR conceived and designed the project. JS performed the experiments and data analysis. TP provided supervision during experimental procedures and the writing process.

Supplement 1 – RPE medium preparation components

Component	Volume (ml)	Final concentration
MEM alpha + Glutamax	91.3	91.3%
Knockout serum	5	5%
N-2 supplement	1	1%
Hydrocortisone, 50 µM	0.11	55 nM
Taurine	0.5	250 µg/ml
Triiodo-L-thyronine (T ₃)	0.07	14 pg/ml
Gentamicin, 50 mg/ml	0.05	25 µg/ml

Supplement 2 – Primary- and secondary antibodies + fluorescent dyes used during immunostainings

Catalog number	Manufacturer	Type	Species	Concentration
Primary antibodies				
610182	BD transduction lab	E-cadherin	Mouse	1/20
DP-1	Progen	Desmoplakin	Guinea pig	1/500
TROMA-I	Developmental Studies Hybridoma bank	Keratin-8	Rat	/
3671	Cell Signaling	pMLC	Rabbit	1/50
9718	Cell Signaling	Γ-H2Ax	Rabbit	1/100
Sc-32909	Santa Cruz	MRTFA	Rabbit	1/100
555719	BD Pharmingen	Integrin beta 4	Rat	1/100
O4886	Sigma	Opsin	Mouse	1/250
Secondary antibodies				
A21235	Molecular Probes	Anti-mouse AF647	Goat	1/100
111-605-144	Hackson/Dianova	Anti-rabbit AF647	Goat	1/100
A-11073	Invitrogen	Anti-guinea pig AF488	Goat	1/500
A21247	Thermo Fisher	Anti-rat AF647	Goat	1/250
712-546-153	Jackson/Dianova	Anti-rat AF488	Donkey	1/250
A-21434	Invitrogen	Anti-rat AF555	Goat	1/250
A-21435	Molecular Probes	Anti-guinea pig AF555	Goat	1/250
Fluorescent dyes				
Ab176753	Abcam	Phalloidin AF488	/	1/100
A12380	Molecular Probes	Phalloidin AF568	/	1/100
H3570	Thermo Fisher Invitrogen	33342 Hoechst	/	1/300



Supplement 3 – DMA-derived data at 1, 4, and 10 Hz. (A) Storage-, loss modulus, and Tan Delta of 1Hz DMA nanoindentation. (n=3). (B) Storage-, loss modulus, and Tan Delta of 4Hz DMA nanoindentation (n=3). (C) Storage-, loss modulus, and Tan Delta of 10Hz DMA nanoindentation (n=3). Error bars are indicated as mean with standard deviation. ANOVA with multiple comparison was used to determine significance. * indicates casp8 vs. GFP. * p ≤ 0.05, ** p ≤ 0.01. 5% significance was applied.